

The impact of passband characteristics on imaging microwave radiometer brightness temperatures over the ocean

Michael H. Bettenhausen¹ and Ian S. Adams¹

Received 30 October 2012; revised 14 May 2013; accepted 17 May 2013; published 21 June 2013.

[1] Radiative transfer modeling is used to estimate the effects of nonideal receiver frequency passband characteristics on the measured brightness temperatures from imaging microwave radiometers over the ocean. The analysis includes microwave frequencies from 6 to 40 GHz and applies to the lower frequency channels of conically scanning, space-based radiometers such as AMSR-E, SSMI, SSMIS, and WindSat. The analysis demonstrates that frequency passband characteristics can have significant effects on the brightness temperatures for microwave imaging channels. The largest effects are due to shifts in the center frequency of the passband. The imaging channels near the water vapor resonance at 22.235 GHz are most sensitive to passband characteristics. The effects for these channels depend on the water vapor in the scene.

Citation: Bettenhausen, M. H., and I. S. Adams (2013), The impact of passband characteristics on imaging microwave radiometer brightness temperatures over the ocean, *Radio Sci.*, 48, 352–357, doi:10.1002/rds.20041.

1. Introduction

[2] Measurements from imaging microwave radiometers over the ocean are used to retrieve a broad range of environmental parameters including sea surface temperature, ocean surface wind speed and direction, total precipitable water vapor, cloud liquid water path, sea ice, and precipitation. The measurements are also assimilated into numerical weather prediction models. Physically based retrieval algorithms and data assimilation of the radiances or brightness temperatures require accurate geophysical modeling of the measurements.

[3] The brightness temperature measured by a radiometer can be expressed as

$$T_b = \frac{\int_0^\infty d\nu T_{b,\nu} H_\nu}{\int_0^\infty d\nu H_\nu} \quad (1)$$

where T_b is the measured brightness temperature, $T_{b,\nu}$ is the incident brightness temperature at the antenna at frequency ν , and H_ν is the receiver passband response at frequency ν . Several fast radiative transfer modeling methods [Lipton *et al.*, 2009; Rosenkranz, 1995, 2003; Saunders *et al.*, 1999; Matricardi *et al.*, 2004; Kleespies *et al.*, 2004] have been developed to approximate (1). Analyses of the accuracy of these methods for frequencies below 40 GHz often assume that H_ν is an idealized rectangular filter centered about the nominal center frequency of the radiometer passband.

[4] We studied the effects of nonideal frequency passband characteristics on the measured brightness temperatures from imaging microwave radiometers for microwave frequencies from 6 to 40 GHz. This frequency range applies to the lower frequency channels of conically scanning, space-based radiometers including Special Sensor Microwave Imager (SSMI) [Hollinger *et al.*, 1990], Advanced Microwave Scanning Radiometer on the EOS platform (AMSR-E) [Kawanishi *et al.*, 2003], Special Sensor Microwave Imager/Sounder (SSMIS) [Kunkee *et al.*, 2008], and WindSat [Gaiser *et al.*, 2004]. We further restricted our analysis to nonprecipitating ocean scenes where the required calibration and modeling accuracy of the brightness temperature is on the order of 1 K or less.

2. Analysis Method

[5] We approximated (1) by evaluating H_ν and $T_{b,\nu}$ at small intervals in ν over the receiver passband and by integrating using the trapezoidal rule. This is similar to the method used to analyze the SSMIS upper air sounding channels by Swadley *et al.* [2008]. We considered passbands at the WindSat nominal center frequencies of 6.8, 10.7, 18.7, 23.8, and 37.0 GHz and the SSMIS nominal center frequency of 22.235 GHz. The small differences between these center frequencies and those used for other instruments such as AMSR-E or the 19.35 GHz channels on SSMIS do not significantly affect the analysis. We used intervals of 10 MHz for the 18.7 and 23.8 GHz passbands, 2 MHz for the 22.235 MHz passband, and 20 MHz for the other passbands. Neglecting ocean surface roughness effects which is appropriate for a surface wind speed of zero, the monochromatic brightness temperature can be written as

$$T_{bp,\nu} = T_{up,\nu} + \tau_\nu [e_{p,\nu} T_S + r_{p,\nu} (T_{down,\nu} + \tau_\nu T_{c,\nu})] \quad (2)$$

¹Remote Sensing Division, Naval Research Laboratory, Washington, D. C., USA.

Corresponding author: M. H. Bettenhausen, Remote Sensing Division, Naval Research Laboratory, Washington, DC 20375, USA. (bettenhausen@nrl.navy.mil)

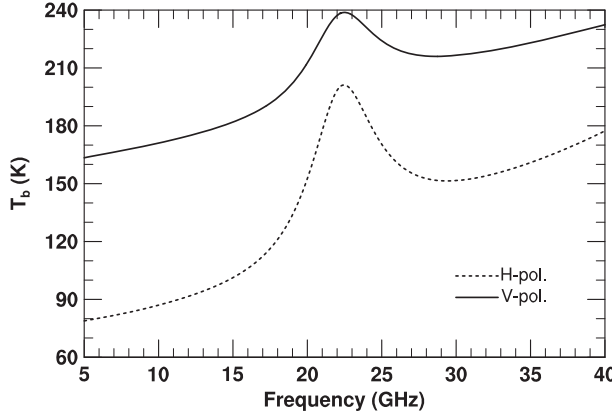


Figure 1. Calculated vertical and horizontal polarization monochromatic brightness temperatures for an atmospheric profile with PWV = 35.4 mm and CLW = 0.15 mm.

where $T_{bp,v}$ and $e_{p,v}$ are the brightness temperature and sea surface emissivity for polarization p at frequency v , $T_{up,v}$ and $T_{down,v}$ are the effective temperatures for atmospheric upwelling and downwelling over the atmospheric profile, T_s is the sea surface temperature, τ_v is the atmospheric transmissivity, $T_{c,v}$ is the cosmic background temperature and $r_{p,v} = (1 - e_{p,v})$. The brightness temperature was calculated using the approximation that the Planck function is a linear function of temperature, which is sufficiently accurate for the frequencies considered [Stogryn, 1975]. The contribution to the emissivity from ocean surface roughness effects is smaller than the specular contribution and also is insensitive to the changes in frequency over a receiver bandwidth [Meissner and Wentz, 2012]. This justifies neglecting the contribution of ocean surface roughness for the present analysis.

[6] We used a set of atmospheric profile databases assembled by the Satellite Application Facility for Numerical Weather Prediction (NWP SAF) [Chevallier *et al.*, 2006]. The profiles comprise parameters at 91 pressure levels as simulated by the European Centre for Medium-Range Weather Forecasts system, and each database provides a diverse set of temperature, humidity, ozone, cloud, or precipitation profiles. We utilized the temperature, water vapor, cloud liquid water profiles, and sea surface temperatures from these databases to assemble an appropriate data set for our analysis including only profiles from the databases compiled to sample temperature, water vapor, and cloud liquid water. Profiles with significant precipitation, determined based on integrated cloud liquid water of greater than 0.3 mm, were excluded along with profiles with non-ocean surface types. The resulting set included a total of 4435 profiles.

[7] The atmospheric parameters $T_{up,v}$, $T_{down,v}$, and τ_v for each atmospheric profile and each frequency were calculated using the monochromatic radiative transfer model MonoRTM [Payne *et al.*, 2011] developed by the Atmospheric and Environmental Research, Inc. MonoRTM has been extensively validated for the microwave frequency range of interest in this paper. Ocean surface emissivities were calculated from the Fresnel reflectivities for a specular sea surface using a parameterization of the permittivity of

sea water developed by Stogryn [1997]. The earth incidence angle (EIA) was set to 54° for all calculations. Changes in the EIA over the range typically used for conically scanning radiometers (50–56°) have a small effect on the frequency sensitivity.

3. Results

[8] Figure 1 shows the calculated brightness temperatures for both vertical and horizontal polarizations for one atmospheric profile. The vertically integrated values for precipitable water vapor (PWV) and cloud liquid water (CLW) for this profile are 35.4 mm and 0.15 mm, respectively, and the corresponding sea surface temperature (SST) is 19.3 K. Water vapor absorption near the 22.235 GHz water vapor resonance is clearly the dominant effect on the spectral characteristics of the brightness temperatures.

[9] Table 1 gives values of the derivative of the monochromatic brightness temperature with respect to frequency ($\partial T_{b,v}/\partial v$) for five different profiles as a measure of the sensitivity of the brightness temperature to changes in frequency. The table includes $\partial T_{b,v}/\partial v$ values for both the vertical and horizontal polarizations and also includes PWV and CLW for each profile and the corresponding SST. The same set of five profiles were used to calculate $\partial T_{b,v}/\partial v$ at each of the five frequencies shown in the table. Results are not shown for 22.235 GHz, because $\partial T_{b,v}/\partial v$ does not provide a good measure of the frequency sensitivity over a receiver passband due to the nonlinearity near the local

Table 1. $\partial T_b/\partial v$ for Vertical and Horizontal Polarizations for Five Different Atmospheric Profiles^a

v_0 (GHz)	SST (°C)	PWV (mm)	CLW (mm)	$\partial T_{b,v}/\partial v$ (K/GHz)	
				V-pol	H-pol
6.8	-1.2	10.9	0.00	1.7	1.2
	16.4	10.9	0.00	1.1	0.8
	-1.9	10.9	0.19	2.1	1.7
	26.3	60.7	0.00	1.4	1.5
	29.5	60.6	0.21	1.7	1.9
10.7	-1.2	10.9	0.00	2.0	1.6
	16.4	10.9	0.00	1.2	1.1
	-1.9	10.9	0.19	2.4	2.2
	26.3	60.7	0.00	1.8	2.3
	29.5	60.6	0.21	2.0	2.9
18.7	-1.2	10.9	0.00	3.9	5.6
	16.4	10.9	0.00	3.5	5.3
	-1.9	10.9	0.19	4.1	6.1
	26.3	60.7	0.00	12.0	20.8
	29.5	60.6	0.21	11.0	19.7
23.8	-1.2	10.9	0.00	-2.1	-6.0
	16.4	10.9	0.00	-3.2	-7.6
	-1.9	10.9	0.19	-1.6	-4.9
	26.3	60.7	0.00	-10.8	-21.6
	29.5	60.6	0.21	-9.1	-18.9
37.0	-1.2	10.9	0.00	1.7	2.8
	16.4	10.9	0.00	1.8	2.8
	-1.9	10.9	0.19	1.8	3.2
	26.3	60.7	0.00	1.8	2.9
	29.5	60.6	0.21	1.8	3.2

^aThe same profiles are used for passbands with five different center frequencies.

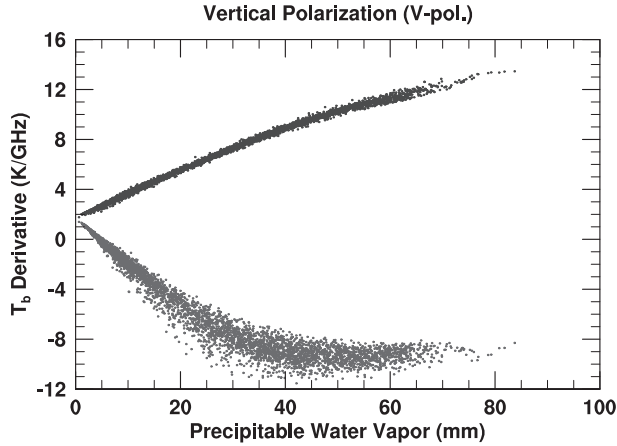


Figure 2. $\partial T_{b,v}/\partial\nu$ for vertical polarization for the full set of profiles plotted versus the vertically integrated precipitable water vapor for each profile. The upper grouping of points is for $\nu_0 = 18.7$ GHz and the lower grouping of points is for $\nu_0 = 23.8$ GHz.

maximum of $T_{b,v}$ as shown in Figure 1. The results in the table show that $T_{b,v}$'s sensitivity to changes in frequency is substantially larger at 18.7 and 23.8 GHz than at the other three frequencies. For example, for the fourth profile, a 10 MHz shift in ν_0 produces an H-pol brightness temperature change of about 0.2 K for both 18.7 and 23.8 but less than 0.03 K for the other passbands. The sensitivities at 18.7 and 23.8 GHz is due to the increase in water vapor absorption as the frequency approaches the water vapor resonance at 22.235 GHz.

[10] Figure 2 is a scatter plot of the calculated values of $\partial T_{b,v}/\partial\nu$ at the nominal center frequencies versus PWV for vertical polarization. Each point is the result for one profile in the set of atmospheric profiles. These results demonstrate the strong dependence of $\partial T_{b,v}/\partial\nu$ on PWV. Figure 3 displays results for horizontal polarization for the same conditions. The only significant difference between the results for the vertical and horizontal polarizations is that the magnitude of $\partial T_{b,v}/\partial\nu$ is larger for horizontal polarization.

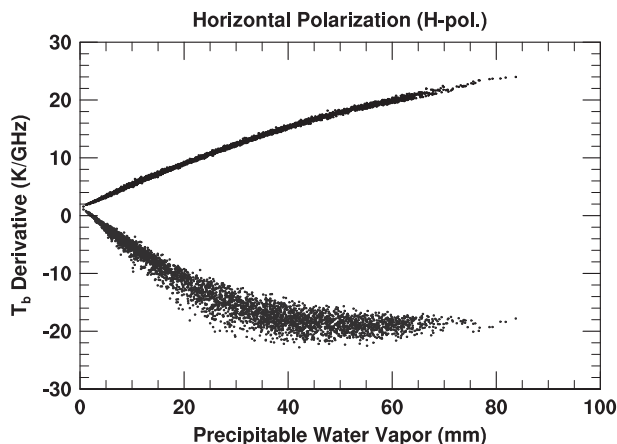


Figure 3. Same as in Figure 2 except for horizontal polarization.

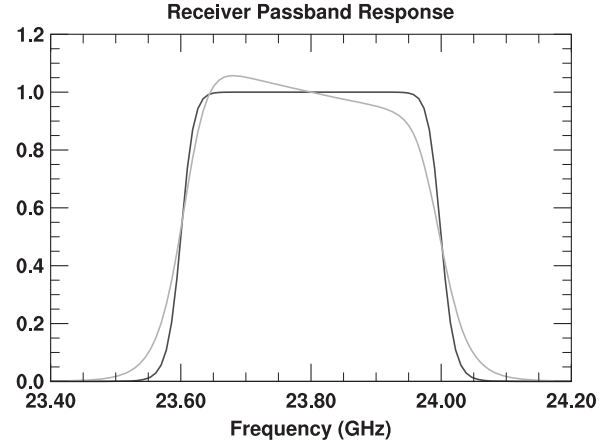


Figure 4. Two examples for H_ν , as given in equation (3), for $\nu_0 = 23.8$ GHz and $B = 400$ MHz: (1) $\alpha = 20, a = 0$ shown in black and (2) $\alpha = 10, a = 0.5$ shown in gray.

The remainder of the results discussed here are for horizontal polarization at 18.7 and 23.8 GHz, where effects of the passband characteristics are strongest as shown by the results in Table 1 and Figures 2 and 3, and for the horizontal polarization at 22.235 GHz.

[11] Equation (1) was evaluated for each profile in the data set using an assumed receiver passband described by

$$H_\nu = \frac{(B/2)^\alpha}{|\nu - \nu_0|^\alpha + (B/2)^\alpha} \left[1 + a \frac{(\nu - \nu_0)}{(10^9 \text{ Hz})} \right] \quad (3)$$

where ν_0 is the nominal center frequency, B is the bandwidth, and $a \neq 0$ simulates a passband that is asymmetric about ν_0 . H_ν , a , and α are dimensionless and B , ν , and ν_0 are in Hz. The α parameter controls the steepness of the decrease in H_ν near $|\nu - \nu_0| = B/2$. An idealized rectangular filter function can be approximated with $a = 0$ and a sufficiently large value of α . Figure 4 shows two example passbands. A cubic hermite polynomial interpolation in frequency of $T_{bp,v}$ was calculated for each of the five passbands and each profile. The interpolation was used to verify that the frequency interval used to integrate over the passband was sufficiently small and to calculate $\partial T_{b,v}/\partial\nu$.

[12] Figure 5 is a scatter plot of the differences between the monochromatic T_{b,ν_0} and T_b calculated using (1) for horizontal polarization with $\nu_0 = 18.7$ GHz. Each point is the difference for a chosen bandwidth and one profile in the set of atmospheric profiles. Figures 6 and 7 show the analogous results for ν_0 equal to 22.235 GHz and 23.8 GHz, respectively. Bandwidth changes have no impact on the measured brightness temperature for a symmetric H_ν if the spectral variation of $T_{b,v}$ is linear. The differences shown in Figures 5–7 are due to the nonlinear variation of the water vapor absorption over the receiver passband. The effect of changing bandwidth is smaller for ν_0 equal to 23.8 GHz than for ν_0 equal to 18.7 GHz or 22.235 GHz because the $T_{b,v}$ is more linear over the passband. The differences in the linearity over the passbands can be seen in Figure 8, which shows $\partial T_{b,v}/\partial\nu$ for frequencies between 18 GHz and 25 GHz for five different atmospheric profiles from the data set. The five profiles have approximately the same values for PWV and CLW. At 23.8 GHz, $\partial T_{b,v}/\partial\nu$ is near

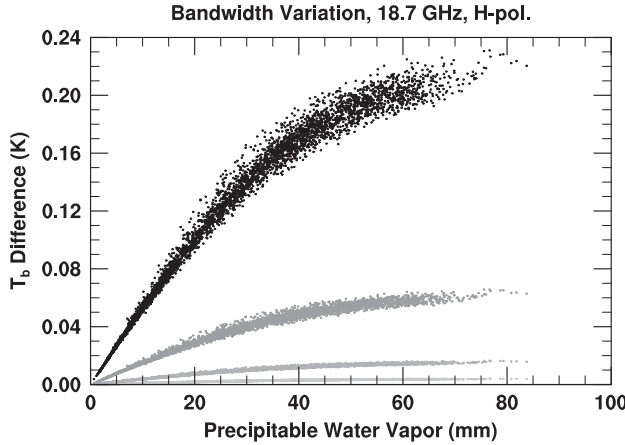


Figure 5. The differences between the monochromatic brightness temperature and brightness temperatures with different bandwidths, ($T_b - T_{b,v_0}$), for horizontal polarization with $a = 0$, $\alpha = 10.0$, and $v_0 = 18.7$ GHz. The bandwidth is varied using values of 100, 200, 400, and 750 MHz with the bandwidth increasing for lighter to darker shade.

a local minimum and is relatively constant over the passband when compared to the changes over the 18.7 GHz and 22.235 GHz passbands. The nonlinearity of the brightness temperature variation with respect to frequency is largest for the 22.235 GHz passband, since it includes a local maximum of $T_{b,v}$ as shown in Figure 1. The $\partial T_{b,v}/\partial v$ differences between the results shown in Figure 8 for the five profiles over the 23.8 GHz passband and at the lower and upper limits of the 22.235 GHz passband indicate significant dependence of $\partial T_{b,v}/\partial v$ on the atmospheric profiles. There is little difference in $\partial T_{b,v}/\partial v$ results for the five different profiles over the 18.7 GHz passband. The greater sensitivity to the atmospheric profile produces greater spread in the results shown in Figures 6 and 7 for the 22.235 GHz and 23.8 GHz passbands than in Figure 5 for the 18.7 GHz passband.

[13] The effect of variations in the parameter α are similar to those from small variations in the bandwidth. As shown in Figures 5–7, changes of the bandwidth on the order of 100 MHz are required to have a significant effect on the calculated brightness temperatures. Realistic variations in the parameter α do not have a significant effect on the calculated brightness temperatures for microwave imaging channels.

[14] Figure 9 is a scatter plot of the difference ($T_{ba_1} - T_{ba_0}$) calculated using (1) for horizontal polarization with $v_0 = 18.7$ GHz. The asymmetry factor, a is -0.5 and 0.0 , respectively, for T_{ba_1} and T_{ba_0} . The bandwidth is consistent for each difference. The difference is negligible for a bandwidth of 100 MHz or less. Figure 10 shows results for the same conditions for the 22.235 GHz passband. $T_{b,v}$ is strongly asymmetric about the center frequency for the 18.7 GHz passband which leads to a significant impact on the integrated brightness temperature. $T_{b,v}$ is more symmetric about the center frequency for the 22.235 GHz passband so the effect of an asymmetric receiver passband is reduced.

[15] Figure 11 shows the effect of asymmetry variation with a fixed bandwidth of 400 MHz for horizontal polarization at 18.7 GHz. The points in the scatter plot are the difference ($T_{ba_1} - T_{ba_0}$) where the asymmetry factor (a) is

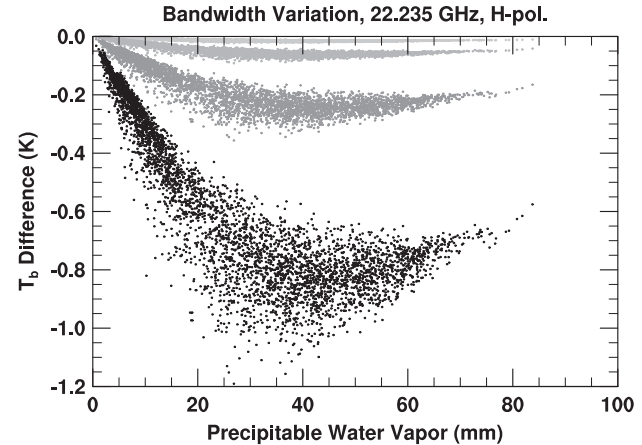


Figure 6. Same as in Figure 5, except for $v_0 = 22.235$ GHz.

zero for T_{ba_0} . Results for 23.8 GHz corresponding to the results shown in Figures 9 and 11 are similar but of the opposite sign. The sign changes because the water vapor absorption increases with decreasing frequency for frequencies above the water vapor resonance at 22.235 GHz and the dependence is the opposite for frequencies below the resonance.

4. Discussion

[16] The results in the previous section demonstrate that the receiver frequency passband characteristics can have significant effects on the brightness temperatures for microwave imaging channels. The largest effects are due to shifts in the center frequency of the passband. The shape of the passband as modeled with the asymmetry factor, a , in (3) is less important but can be significant especially for larger bandwidths. The imaging channels that are most sensitive to passband characteristics are those near the water vapor resonance at 22.235 GHz. The effects for these channels depend strongly on the PWV in the scene.

[17] Measurements of the receiver frequency passband characteristics are often not generally available for existing

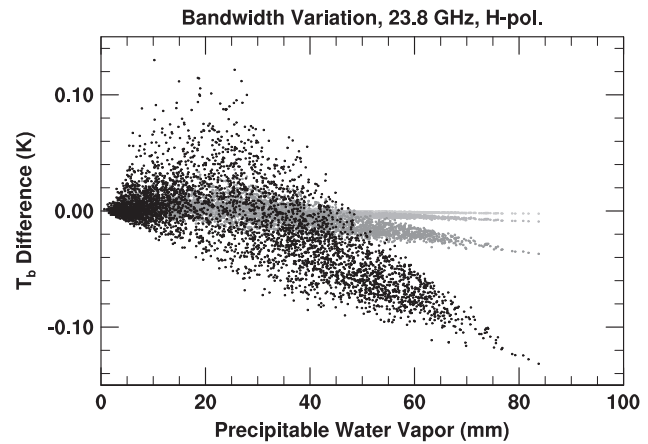


Figure 7. Same as in Figure 5, except for $v_0 = 23.8$ GHz.

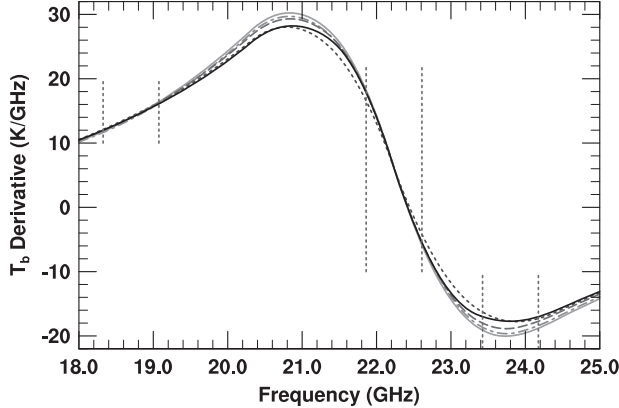


Figure 8. $\partial T_{b,v} / \partial v$ for horizontal polarization for all five profiles from the set of atmospheric profiles for which $34.9 \text{ mm} < \text{PWV} < 35.1 \text{ mm}$ and $\text{CLW} < 0.03 \text{ mm}$. The vertical dashed lines denote 750 MHz wide bands centered around 18.7 GHz, 22.235 GHz, and 23.8 GHz.

and heritage microwave imagers. In these instances, retrieval and data assimilation algorithms typically assume that the receiver passband is an ideal rectangular filter centered on the nominal center frequency. Our results in section 3 show that this can lead to a model bias that depends on PWV. Data products that are sensitive to the difference between polarizations at the same nominal center frequency are most likely to be affected. This would occur if the passband characteristics for the receivers for the two polarizations were mismatched. For example, using the results shown in Figure 3, a model bias of about 0.6 K for a scene with 60 mm PWV would result for vertical and horizontal polarizations at 18.7 GHz and 18.73 GHz, respectively, if both channels were modeled at 18.7 GHz.

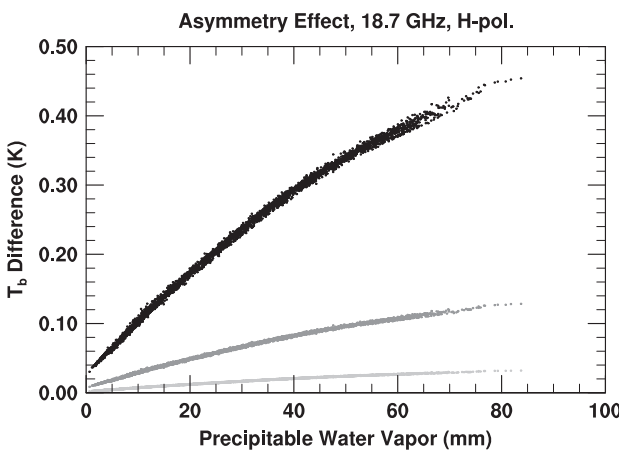


Figure 9. The differences between the calculated horizontal polarization brightness temperatures with a symmetric passband and the brightness temperatures with an asymmetric passband, $a = -0.5$, with $\alpha = 10.0$ and $v_0 = 18.7 \text{ GHz}$. The bandwidth is varied using values of 200, 400, and 750 MHz with the bandwidth increasing from the bottom set of points to the top set of points.

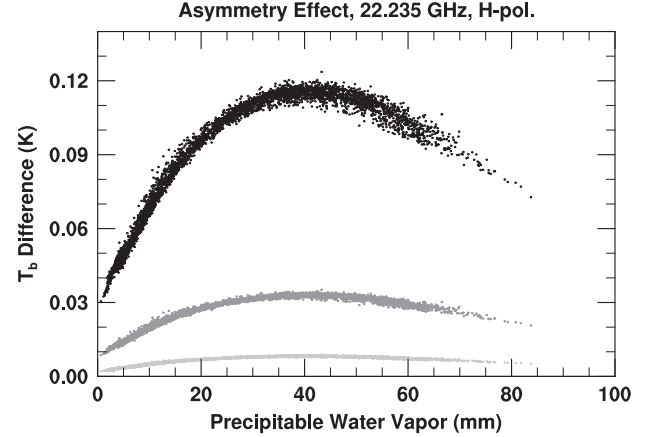


Figure 10. Same as in Figure 9, except for $v_0 = 22.235 \text{ GHz}$.

[18] Receiver passband effects could be even more important for measurement of the third and fourth Stokes components of the brightness temperature formed using polarization differences [Gaiser et al., 2004]. For example, the wind direction retrievals for WindSat are sensitive to changes on the order of 0.1 K in the third and fourth Stokes components [Bettenhausen et al., 2006]. Passband effects could be significant even at frequencies near 10.7 GHz and 37 GHz for these measurements if the passband responses for polarization pairs ($+45^\circ$ and -45° or left and right circular polarizations) differ significantly.

[19] The results in this paper suggest that receiver frequency passband effects should be carefully considered during the design of imaging microwave radiometers. Prelaunch characterization of the passband characteristics and the stability of the passband characteristics over the range of on-orbit operating conditions is important. Significant departures from nominal design parameters

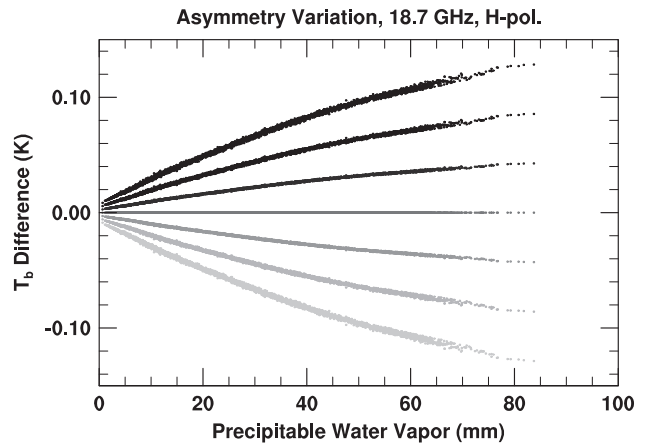


Figure 11. The differences between the calculated horizontal polarization brightness temperatures with a symmetric passband and the brightness temperatures with passbands with various asymmetry factors, $a = [-1/2, -1/3, -1/6, 0, 1/6, 1/3, 1/2]$. The values used for a are increasing from the top to the bottom set of points (darker to lighter shades). Bandwidth is 400 MHz, $\alpha = 10.0$, and $v_0 = 18.7 \text{ GHz}$.

should be incorporated into models for the affected channels. It is important that instrument developers make the measurements of the passband characteristics generally available to the community for radiative transfer modeling.

[20] **Acknowledgment.** This work was supported by the Office of Naval Research.

References

- Bettenhausen, M. H., C. K. Smith, R. M. Bevilacqua, N.-Y. Wang, P. W. Gaiser, and S. Cox (2006), A nonlinear optimization algorithm for WindSat wind vector retrievals, *IEEE Trans. Geosci. Remote Sens.*, *44*(3), 597–610.
- Chevallier, F., S. D. Michele, and A. P. McNally, (2006), Diverse profile datasets from the ECMWF 91-level short-range forecasts, *Tech. Rep. NPWSAF-EC-TR-010*, Satell. Appl. Facil. for Numer. Weather Predict., [Available at http://research.metoffice.gov.uk/interproj/nwpsaf/rtm_profiles_91L.pdf] verified on 2013-06-07.
- Gaiser, P. W., et al. (2004), The WindSat spaceborne polarimetric microwave radiometer: Sensor description and early orbit performance, *IEEE Trans. Geosci. Remote Sens.*, *42*(11), 2347–2361.
- Hollinger, J. P., J. L. Peirce, and G. A. Poe (1990), SSM/I instrument evaluation, *IEEE Trans. Geosci. Remote Sens.*, *28*(5), 781–790.
- Kawanishi, T., T. Sezai, Y. Ito, K. Imaoka, T. Takeshima, Y. Ishido, A. Shibata, M. Miura, H. Inahata, and R. W. Spencer (2003), The Advanced Microwave Scanning Radiometer for the Earth Observing System AMSR-E, NASA's contribution to the EOS for global energy and water cycle studies, *IEEE Trans. Geosci. Remote Sens.*, *41*(2), 184–194.
- Kleespies, T. J., P. van Delst, L. M. McMillin, and J. Derber (2004), Atmospheric transmittance of an absorbing gas. 6. OPTRAN status report and introduction to the NESDIS/NCEP community radiative transfer model, *Appl. Opt.*, *43*(15), 3103–3109, doi:10.1364/AO.43.003103.
- Kunkee, D., G. Poe, D. Boucher, S. Swadley, Y. Hong, J. Wessel, and E. Uliana (2008), Design and evaluation of the first special sensor microwave imager/sounder, *IEEE Trans. Geosci. Remote Sens.*, *46*(4), 863–883, doi:10.1109/TGRS.2008.917980.
- Lipton, A., J.-L. Moncet, S.-A. Boukabara, G. Uymin, and K. Quinn (2009), Fast and accurate radiative transfer in the microwave with optimum spectral sampling, *IEEE Trans. Geosci. Remote Sens.*, *47*(7), 1909–1917, doi:10.1109/TGRS.2008.2010933.
- Matricardi, M., F. Chevallier, and G. Kelly (2004), An improved general fast radiative transfer model for the assimilation of radiance observations, *Q. J. R. Meteorol. Soc.*, *130*(596), 153–173, doi:10.1256/qj.02.181.
- Meissner, T., and F. J. Wentz (2012), The emissivity of the ocean surface between 6 and 90 GHz over a large range of wind speeds and earth incidence angles, *IEEE Trans. Geosci. Remote Sens.*, *50*(8), 3004–3026, doi:10.1109/TGRS.2011.2179662.
- Payne, V., E. Mlawer, K. Cady-Pereira, and J. Moncet (2011), Water vapor continuum absorption in the microwave, *IEEE Trans. Geosci. Remote Sens.*, *49*(6), 2194–2208, doi:10.1109/TGRS.2010.2091416.
- Rosenkranz, P. (1995), A rapid atmospheric transmittance algorithm for microwave sounding channels, *IEEE Trans. Geosci. Remote Sens.*, *33*(5), 1135–1140, doi:10.1109/36.469477.
- Rosenkranz, P. (2003), Rapid radiative transfer model for AMSU/HSB channels, *IEEE Trans. Geosci. Remote Sens.*, *41*(2), 362–368, doi:10.1109/TGRS.2002.808323.
- Saunders, R., M. Matricardi, and P. Brunel (1999), An improved fast radiative transfer model for assimilation of satellite radiance observations, *Q. J. R. Meteorol. Soc.*, *125*(556), 1407–1425, doi:10.1002/qj.1999.49712555615.
- Stogryn, A. (1975), A note on brightness temperature at millimeter wavelengths, *IEEE Trans. Geosci. Elect.*, *13*(2), 81–84, doi:10.1109/TGE.1975.294380.
- Stogryn, A. P. (1997), Equations for the permittivity of sea water, report, Nav. Res. Lab., Washington, D. C.
- Swadley, S., G. Poe, W. Bell, Y. Hong, D. Kunkee, I. McDermid, and T. Leblanc (2008), Analysis and characterization of the ssmis upper atmosphere sounding channel measurements, *IEEE Trans. Geosci. Remote Sens.*, *46*(4), 962–983.